Chapter 1

General Introduction

1.1 Polymer-Metal Complexes and their Functions

Organic polymers provide with unique properties, such as good mechanical strength and processibility, light weight, and so on. They are part of our daily life, and sometimes it is pointed out based on their broad applications, that we are living now in the so−called “plastic time” or “polymeric time”. But organic polymers are generally in some way limited by the relatively low thermal stability and not well−pronounced possibility for important processes, such as binding interaction of small molecules, electron transfer processes, therapeutic effects.[1-2] Therefore, development of new materials is of fundamental importance.

There has been growing attention to the molecular functions of polymer-metal complexes as a new frontier in material science. Because the complexes are combinations of polymers and metal compounds at the molecule or nanometer level and are structurally labile, there are unlimited possibilities for providing a wide variety of previously unknown molecular functions.

1.1.1 Structure features of polymer-metal complexes

A polymer-metal complex is composed of a polymer and metal compound in which the metal compound is incorporated to the polymer by various modes. Metal compounds can be included either as metal salts, metal complexes, metal chelates, or metal clusters.[2]

Although polymer-metal complexes are involved in various processes for life and essential on earth, e.g. oxygen transport in blood by hemoglobin, the first publication of polymer-metal complexes for improving the thermostability appeared in the late Fifties and early Sixties.[3-4] In the early Seventies an increase of studies were concerned with catalytic properties of polymer bound metal complexes with the aim to heterogenize homogeneous catalysts for various chemical reactions.[5-6] At the end of the Seventies and beginning of Eighties the studies about binding of small molecules and conversion of solar energy by using polymer-metal complexes started.[7-8] The most recent development is the formation and stabilization of metal nanoparticles/clusters (1−100

nm) in polymers. This direction leads to new composite materials with several interesting properties. [9-10]

Polymer-metal complexes can be classified into three main groups considering the "chemical" binding of metal compounds (MXn) to suitable polymer ligands or higher functional ligands. Figure 1 to 3 schematically shows possible combinations of polymers with metal compounds.

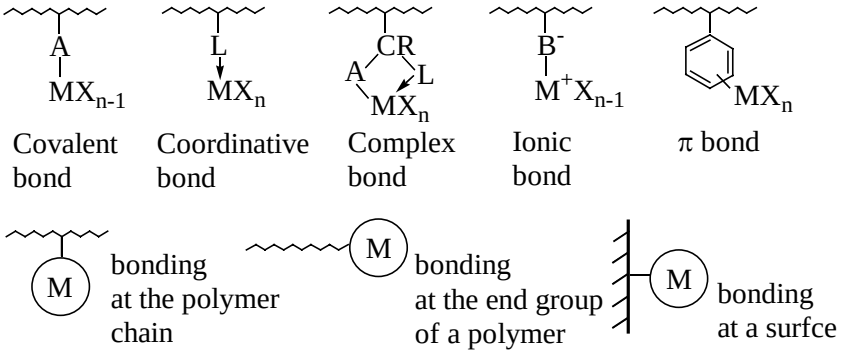

Figure 1. Metal compounds bound at a chain or a surface of polymers (*Type I*).

In *Type I* a metal compound is bound to a chain of a linear or crosslinked polymer or a surface of the polymer via a covalent, a coordinative, a complex (at the ligand of a complex), an ionic or a π–bond (Figure 1).

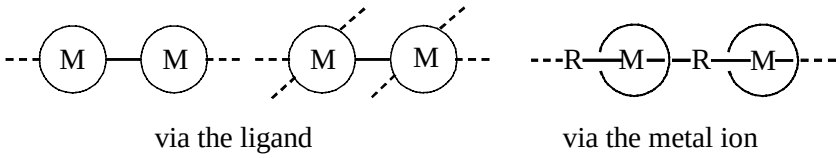

Figure 2. Metal compounds as part of a polymer chain or network (*Type II*).

In *Type II* the bifunctional or high functional ligand and the metal compound are part of a polymer chain or network via the ligand or the metal ion (Figure 2).

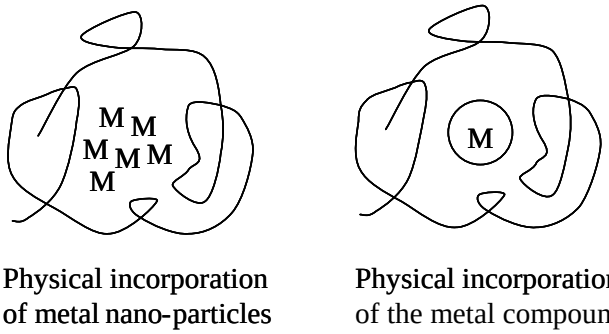

Figure 3. Physical incorporation of the metal compound in polymers (*Type III*).

In *type III* (Figure 3) metal nanoparticles or the metal compound physically incorporated in polymers.

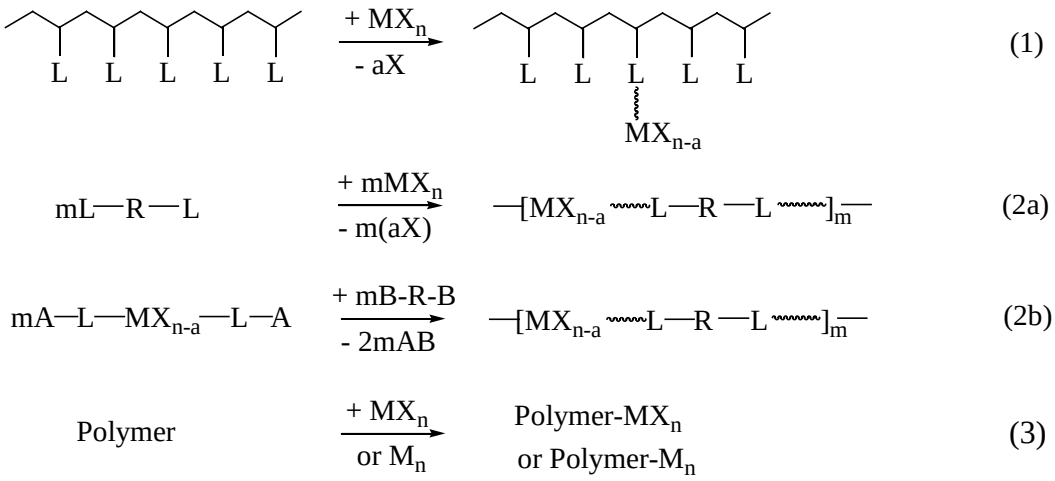

Figure 4. Formation of various polymer-metal complexes.
((1) *type I*, (2a, 2b) *type II*, (3) *type III*))

Figure 4 shows the fundamentals for the formation of polymer-metal complexes.[11] Polymers or polymer ligands that were applied to complex with metal compounds can be classified as protic (e.g., -OH, -COOH, >NH, -NH_2, >PH, $RO(OH)_2$, -SH, -C(S)OH, -C(S)SH.), and aprotonic types (groups or heteroatoms with unpaired free electron pairs capable of donor-acceptor or π-interaction with MX_n, such as >C=O, -COOR, -N=O, -NO_2, -N=N-, >C=S, -CN, >C=C<, -SCN, -PR_2.).[12-13]

Typical examples of polymer ligands are presented in figure 5. Polymer ligands contain anchoring sites like nitrogen, oxygen or sulphur obtained either by the polymerization of monomer possessing the coordinating site or by chemical reactions between polymers and low molecular weight compounds having the coordinating ability. For example, poly(vinyl pyridine)s, poly(vinyl amine)s, poly(acrylic acid)s, polythiols as homo- or copolymers, have a high affinity to coordinate metals, such as Zn, Ni, Co, Ru, Pd, and their compounds.[14-16] The type and strength of the formed M-L bonds depend on the ionization potential and electron affinity of the transition metal ion as well as the distance between the charges.

Composition and structure of polymer-metal complexes are affected not only by the nature of the metal compound and ligand (L), but also by specific polymer parameters such as degree of cross-linking, distribution of L, and in the case of insoluble polymers, by the topography of the polymer ligand. The process of complex formation is accompanied by numerous complicated factors such as ion exchange

equilibrium, ligand conformational changes, influence of change in electrostatic surface potential, etc. Therefore, the ratio of metal to ligand for polymer complexes is of more significance in comparison with that for soluble low molecular weight metal complexes.

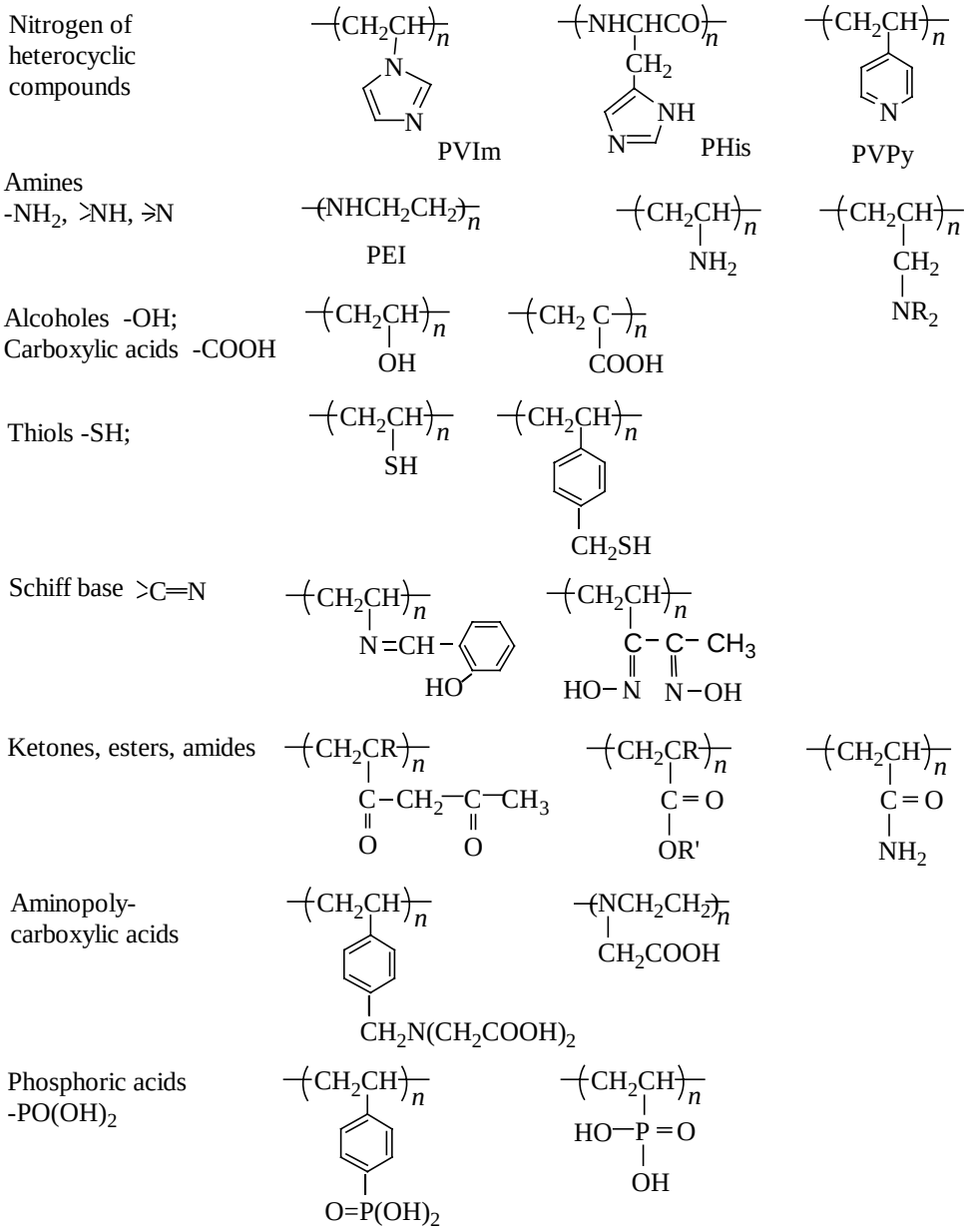

Figure 5. Typical polymer ligands for polymer-metal complexes.

The formation of a polymer-metal complex is in general thermodynamically favored by a negative free energy. The so-called polymer chelate effect (change of the free energy due to the addition of a metal compound to a polymer ligand) gives an additional contribution comparing with the known “chelate effect” for the formation of low molecular weight metal complexes. Because of local, molecular and supramolecular

organization of polymers that may be changed by formation of a polymer-metal complex, the situation is much more complicated in comparison with low molecular weight analogs.

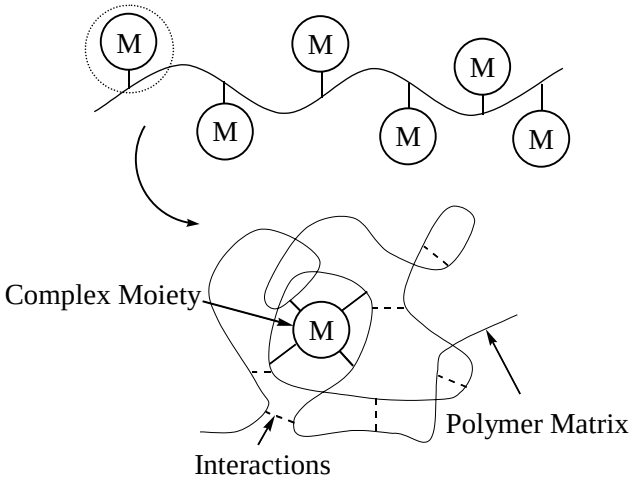

Figure 6. Schematic representation of a conformational change of the polymer-metal complexes.

In polymer-metal complexes, physicochemical properties and chemical reactivities of the complex moieties are often strongly affected by interactions with the polymers, which surround the complex moieties as illustrated in Figure 6. At linear organic polymers the secondary bonding forces of a bound metal to other part are weak, such as coordination bonds, hydrogen bonds, charge-transfer interaction, hydrophobic interaction and so forth. But these interactions act multiply and dynamically. The polymers also provide specific microenvironments around the complex moieties that contribute to regulation of the electronic state in the complex moieties. An integrated structure or a sequential structure of the complex moieties brings about new concepts of the multielectron transfer step and sequential field, which also characterize the polymer-metal complexes.[2]

1.1.2 Functions and potential applications of polymer-metal complexes

In nature, different polymer-metal complexes regulate energy conversion in photosynthesis, multi-electron transfer and catalysis in cofactors and metalloenzymes, gas transport in blood and other processes.[2] A typical example is the efficient oxygen transport by hemoglobin in blood, which is a conjugated protein that has an iron-porphyrin as the oxygen-binding site. On exposure of the hemoglobin solution to oxygen, the iron-porphyrin is converted to its oxygen-bound form. This oxygen-binding reaction is rapid and reversible in response to oxygen partial pressure, as represented in

Eq. 4. The oxygen-binding equilibrium constant (*K*) is moderate for hemoglobin to deliver oxygen to terminal tissues.[17]

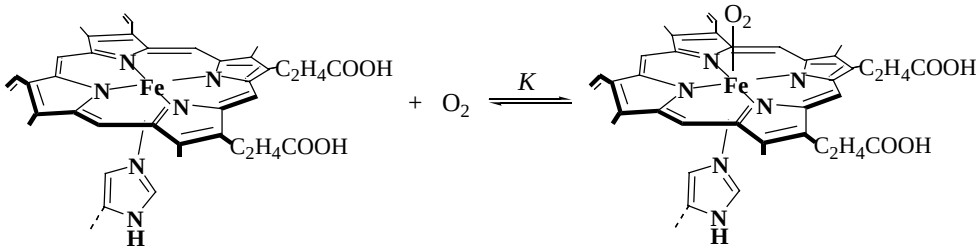

(4)

Synthetic polymer-metals complexes are today of increasing interest as catalysts, conductors, photoconductors, interaction with small molecules, sensors, electron/photoelectron induced processes, magnetic materials, medical materials. Table 1 shows the properties and potential applications of polymer-metal complexes.[2]

Table 1. Properties and potential applications of polymer-metal complexes.

Properties	Potential applications
Selectivity	Gas transport, separation, sensor
Mixed valence solution systems	Multielectron transfer, catalysis, photocatalysis, artificial photosynthesis, electrochemistry
Solid-state photon interactions	Photovoltaic cell, photoelectrochemistry, electroluminescence, optical information storage
Electron, photoelectron conduction	Molecular devices, photoconductors, lasergraphy, electrochemistry
Ionic conduction	Electron-capture-detector devices, superconductors, polymer battery
Nonlinear optical effect	Modulator, integrated optics, high-power laser
Therapeutic effect	Drugs, photodrugs
Preceramics	Thermally stable compounds, quantum devices

Catalysis The metal ions attached to the polymer backbone are bound to exhibit characteristic catalytic behavior. The catalytic cycle of a polymer-metal complex is illustrated in Eq. 5, where M is the metal ion, L is the ligand, and S is the substrate.

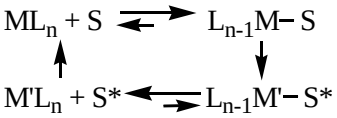

(5)

In the first step the substrate coordinates to a catalyst molecule, forming an intermediate mixed complex. The substrate is then activated by metal ions and dissociates from the catalyst. The complex catalyst, having accomplished its purpose, is regenerated to the original complex. The catalyst action of a metal ion depends

substantially on the nature of the ligands in the intermediate mixed complex.

Table 2. Examples of chemical reactions catalysed by polymer-metal complexes.

Metal	Polymer matrix	Catalytic reaction
Ru, Rh	Phosphenated polystyrene	Isomerization of olefins
Rh	Phosphenated polystyrene	Hydrogenation of olefins
Rh	Phosphenated polystyrene	Synthesis of pyridines
Rh	Phosphenated polystyrene	Hydroformylation of olefins
Pt-Sn	Polymer ligands containing P, N, or S	Hydroformylation of olefins
Ni	Polystyrene with P/O ligands	Polymerization of ethylene
Pd	Nitrile and benzoimidazole bound to various polymers	Oxidation of olefins
Cu	4-vinylpyridine polymers	Oxidation of phenols
Mn, Fe	Poly(pyrroleporphyrin)	Oxidation of olefins and phenols
	Polystyrene with P/O ligands	Oxidation of sulfoxides
	Various ligands	Oxidating polymerisation of disulfides
Nd	Acrylic acid-styrene copolymers	Polymerisation of isoprene

The main goal of the complex catalysts was the preparation of catalytic systems displaying the good activity, selectivity and reproducibility, combined with the easy separability and recovery characteristics of homogeneous catalysts. It is now possible to select the proper system, including polymers and metal derivatives, for a specific purpose related to a certain chemical reaction and process conditions. Indeed, whereas selection of the metal is first of all dependent on the reaction of interest, the selection of the polymer can be made depending on external parameters such as solvent, temperature, reagents, products, and reactor. Table 2 listed the typical metals, polymer matrices, and the corresponding catalytic reactions.[18-19]

In recent years, metal-centred polymeric complexes, such as Fe(II) and Ru(II) complexes with one to three (4,4'-halomethyl)-2,2'-bipyridine (bpy) ligands, have been used to initiate living cationic oxazoline polymerisations. The polymerizations yielded hybrid systems with molecular weights from 1600 to 4600 and low polydispersities.[20-21]

Multielectron transfer Electron transfer also plays a significant role in many chemical reactions, e.g., reduction of oxygen. The thermodynamically allowed potential for the two-electron reduction of oxygen in acidic media is located at 0.68V (vs SHE), where that for the four-electron at 1.23V (vs SHE). The direct electron transfer from the electrode to oxygen in the electrolyte solution is usually kinetically very slow at moderate potentials, and electron mediators are frequently employed to enhance the rate

of electron transfer.

Anson[22-23] reported the formation of the coordination of four $Ru(NH_3)_5^{2+}$ groups to 5,10,15,20-tetrakis(4-pyridyl)porphyrinatocobalt(II) ($CoP(py)_4$, Figure 7). The resulting tetrauthenated complex, $CoP(pyRu(NH_3)_5^{8+})$, is an effective catalyst for the four-electron reduction of oxygen to water.

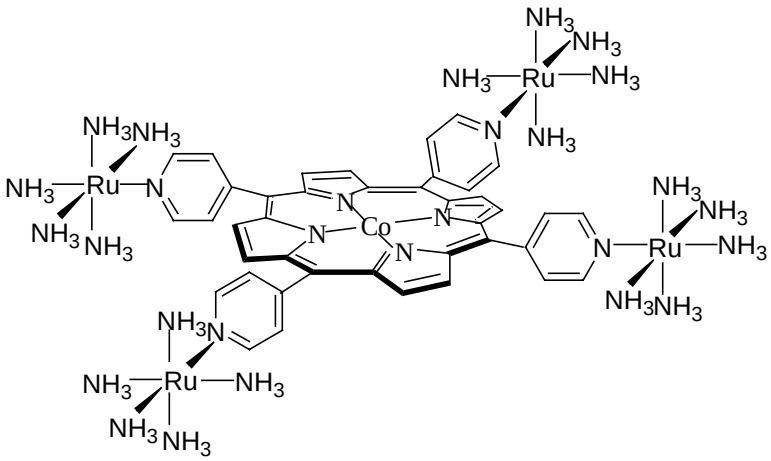

Figure 7. Structure of $CoP(pyRu(NH_3)_5^{8+})$.

Ionic conduction The utilization of flexible solid polymer electrolyte (SPE) is very important to manufacture small batteries and microdevices. Since Wright[24] reported that poly(oxyethylene) (POE)-alkaline metal ion complexes showed ionic conductivities of 10^{-7}-10^{-8} S/cm at ambient temperatures in 1975, various efforts have been made to greatly improve the ionic conductivity of SPE.

The improvement of the performance of SPEs has been carried out along the two approaches: (i) enhancement in the mobility of the polymer chains, and (ii) increase in the metal ion concentration. With the combination of (i) and (ii), the ionic conductivity of SPEs have been greatly improved. Angell[25] and Watanabe[26] announced 10^{-3} S/cm at ambient temperatures.

Although the SPE now shows the ionic conductivity of 10^{-3} S/cm at ambient temperature, but still insufficient in comparison with liquid electrolyte systems, furthermore, SPE tends to crystallize at low temperature, which prevents it from practical application. Therefore, increasing the mobility of polymers and the number of dissociating metal ions, preventing crystallization, is still the future trend. [27] If the problem could be solved, many advantages of polymer materials, such as light weight, thin film-forming ability, flexibility, would lead to new types of electrochemical devices and batteries.

Photosensitive material The polymer-metal complexes could also act as new and

modulable photosensitive materials. Irradiation of polymer-metal complexes, for example in the visible region of light if colored polymer-metal complexes are employed, produce the excited states that can be used for electron transport in photochemical reactions, photoelectrochemcial devices, photovoltaic cells, sensors, etc. The most important photoinduced electron transport exists in photosynthesis of green plants providing almost all the energy sources for biological activities. [29-30]

Photoinduced electron transport in synthetic polymer-metal complexes can be of great help for elucidating the microenviromental effect on the photoprocess by polymer solution, polymer bulk or molecular aggregates. In these systems it was shown that the metal compound can act as the photoexcitaion centre, which is coupled with another electron donor or acceptor, where in other cases the metal compound behaves as electron acceptor/donor in combination with another photoexcitation centre. These aspects are particularly interesting when the metal compound is combined into a polymeric membrane where electronic properties can be modulated and the design of devices can be effective. Solid polymer-metal complexes can have interesting electroconductivity, photoconductivity and nonlinear optical properties, which can be modulated for different applications both at the level of the metal compound and of the polymer matrix.

Separation An important application for the coordination of polymer ligands with metal ions is the extraction of trace amounts of metals. For example, using polymers with amidoxime groups an industrial extraction of uranium from seawater was elaborated.[31]

Also, weak coordination of metal compounds wrapped into polymers could be used for specific and selective separation of small molecules from mixtures where they may be present even in small concentration (see 1.3.2 in detail).

In addition, some of the polymer-metal complexes can be used as high performance molecular devices, such as super conductors, organic ferromagnets, and nonlinear optics.

1.2 Cobalt Complexes and their Oxygen-binding Properties

It is known that metal complexes indicate specific and reversible binding abilities with gaseous molecules, for example, hemoglobin and myoglobin with oxygen in a living body. However, the ironporphyrin isolated from hemoglobin is immediately and irreversibly oxidized to its ferric [iron(III)] form, and it does not act as a reversible oxygen-binding site. While cobaltporphyrins have the high oxidation potential in comparison with ironporphyrins, therefore, cobalt complexes with selective and reversible oxygen-binding ability provide extensive potential applications, such as air

separation membranes, oxygen absorbents, sensors.[2,7,32]

1.2.1 Formation of polymer-cobalt complexes

Polymer-cobaltporphyrin complexes are formed by mixing solutions of a polymer-ligand having nitrogenous residues, such as polymers and copolymers based on vinylpyridines and vinylimidazole with a cobaltporphyrin as schematically shown in Eq. 6, where Co, L, and the ellipse represent a cobalt ion, a ligand such as a nitrogenous residue, and a porphyrin planar ring, respectively.

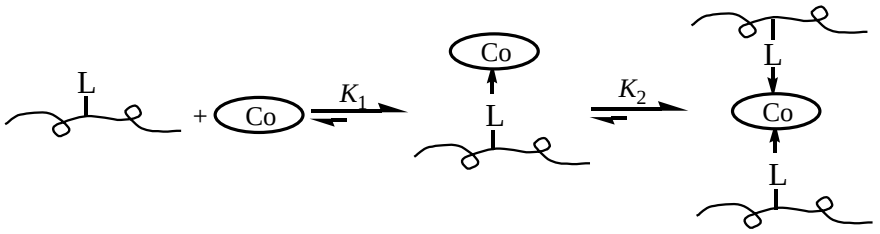

(6)

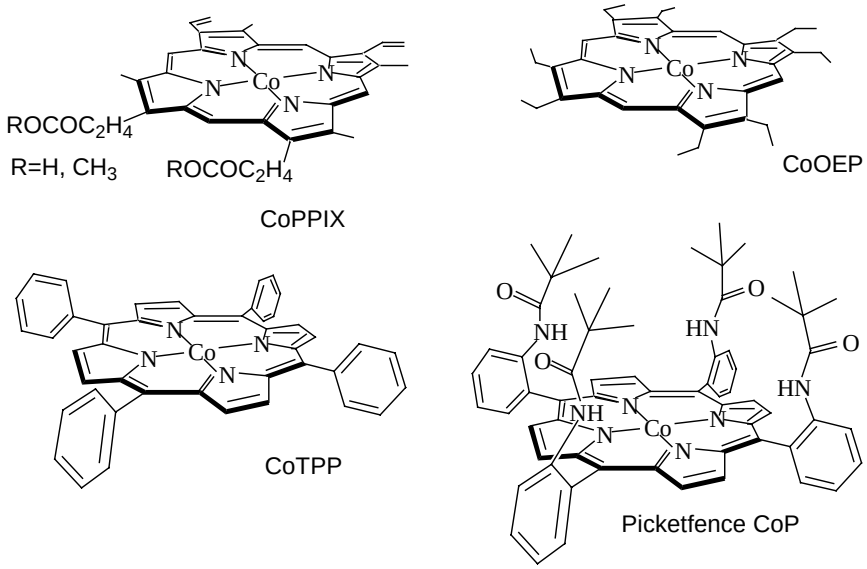

Figure 8. Typical examples of cobaltporphyrins.

Typical examples of cobaltporphyrins are presented in Figure 8. Figolic summarized the detailed information of variuous oxygen carriers based on cobalt.[33] The donor properties of nitrogen-containing polymer ligands are specified by the presence of unshared electron pair at the nitrogen atom localized at sp^2-orbital and conjugated with the unoccupied orbital of cobalt ions. The ligand-coordination in the pendant-type cobaltporphyrin enables the formation of an oxygen-adduct. However, when another ligand further coordinates to the sixth coordination site of the cobaltporphyrin as shown in Eq. 6, the cobaltporphyrin loses the oxygen-binding ability. Consequently, the structure and hence the functions of the cobaltporphyrin are significantly affected by the attachment of polymer ligands.

For a reversible oxygen-binding, the oxidation potential of a cobaltporphyrin must be within a range such that a certain amount of electron density is located to the bound oxygen molecule, yet not so great that irreversible oxidation of the cobalt accompanying the formation of super oxide anion ($O_2^{-\bullet}$) occurs.[7,34-35] An aromatic and nitrogenous ligand, such as imidazole and pyridine, contributes to this requisite, from the viewpoint of an axial ligand of a cobaltporphyrin. The coordination number of one or two, that is, the molar ratio of the coordinated axial ligand to the cobalt ion of porphyrin (Eq. 6), and the formation constants (K_1 and K_2) of cobaltporphyrin-polymer complexes have been well studied by spectroscopic titration.[36] For example, the visible absorption spectrum of a picket-fence cobaltporphyrin (CoP) with λ_{max} = 524 nm changed with the addition of the polymer ligand to the spectrum with λ_{max} = 527 nm assigned to a five-coordinated CoP.[37] In solutions, cobaltporphyrins preferentially form the five-coordinate complexes with almost all the imidazole and pyridine-based ligands with a K_1 value of $10 - 10^3 M^{-1}$. Cobaltporphyrin hardly forms a six-coordinate complex because K_2 for the six-coordinate complex is very small ($<1 M^{-1}$).[38]

Casting the complex solution of a cobaltporphyrin and a polymer-ligand such as poly(vinylimidazole-*co*-alkylmethacrylate) (OIm), for example, on a Teflon plate and drying, yielded both a homogenously dispersed cobaltporphyrin in a solid state and a mechanically tough membrane.[17] The glass transition temperature (T_g) of the membrane was increased, for example, from -1°C for OIm itself to 6°C and the membrane become brittle after the 40 wt.% -incorporation of cobaltporphyrin, which was explained by a hardening effect of the incorporated planar and rigid porphyrin molecules on the segmental motion of the polymer chains.

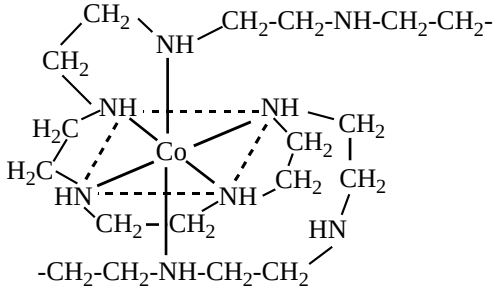

Figure 9. Structure of a (polyethyleneiminato)cobalt complex.

Both linear and branched polyethyleneimine (PEI) show high coordinative ability. The reason lies in the fact that the behavior of repeating –NH-CH_2-CH_2- group is in a first approximation similar to ethylenediamine. The mechanism of the complex formation with PEI has been studied in detail for the case of cobalt salt interactions.[2,39] Coordinative PEI-Co complexes have been formed (Figure 9), and the high coordinative ability of PEI is also conformed by the fact that all ligand groups of cobalt complexes

have been replaced by ethyleneimine units within all the examined reagents concentrations.

1.2.2 Oxygen-binding properties of polymer-cobalt complexes

One of the significant properties of polymer-cobalt complexes is the specific oxygen-binding ability. For example, after the central cobalt ion of cobaltporphyrin was attached to a polymer ligand, the five-coordinate cobaltporphyrin binds molecular oxygen selectively, rapidly, and reversibly (Eq. 7).

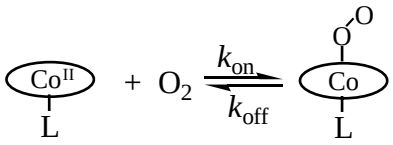

$$K\,(1/p_{50}) = k_{on}/k_{off} \qquad (7)$$

In addition to a five-coordinate cobaltporphyrin formation and its adequate oxidation potential, the following requisites for reversible oxygen-binding have been elucidated to suppress the side-reactions of an oxygen adduct or irreversible oxidations of a cobaltporphyrin, as represented by Eqs. 8 to 10.[7,34]

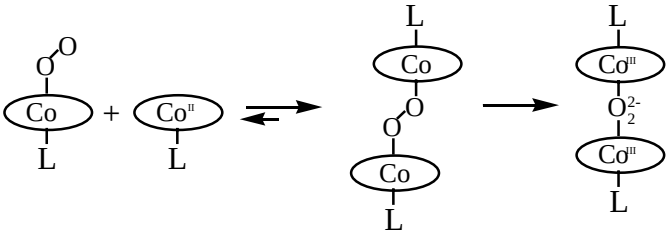

(8)

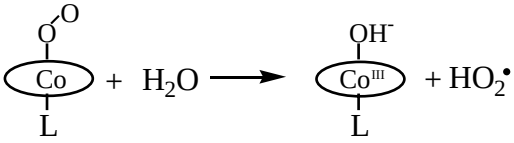

(9)

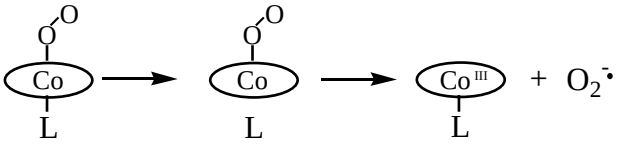

(10)

There is a strong driving force toward the irreversible formation of a stable μ-oxo-Co(III)P dimmer (Eq. 8). The oxygen-bound complex, or oxygen adduct, rapidly reacts with another deoxy Co(II)P, forming a binuclear dioxygen-bridged complex. This binuclear complex is irreversibly converted to an oxo-bridged Co(III) dimer. In other words, the first problem of reversible oxygen-binding is how to inhibit dimerization.

Much work has been concerned with overcoming this problem, and two approaches

have been successful. The first is an elegant steric approach, where a planar porphyrin is sterically substituted in a fashion that inhibits dimerization. A typical example is a *meso*-α,α,α,α-tetrakis(*o*-pivalamidophenyl) porphrinatocobalt (picketfence in Figure 8), which has four pivalamido groups on one side of the porphyrin plane that provide a cavity for protecting the bound oxygen from the dimerization.[32] Another realistic approach is to attach the cobaltporphyrins to a rigid polymer chain to prevent the two cobaltoporphyrins from reacting with each other and dimerizing. By these means, reversible oxygen-binding to cobaltporphyrins has been achieved under limited conditions.

The next requisite is that the proton-driven oxidation (see Eq. 9) has to be retarded with a hydrophobic environment. Hydrophobic polymers are expected to satisfy the requisite.

Another requisite is that the oxidation induced by a ligand-off (see Eq. 10) has to be retarded with a stable five-coordinate complexation. Although a cobaltporphyrin complex with an axial ligand is thermodynamically stable with a large K_1, the cobaltporphyrin is still liable in the ligand complexation. A moment dissociation of the axial ligand in the oxygen-bound complex causes an electron transfer from the cobalt(II) ion to the bound oxygen molecule to yield Co(III)P and a super oxide anion. A stable cobaltporphyrin-polymer complexation with a large K_1 value has been characterized in comparison with the monomeric complexes. For these reasons, cobaltporphyrin-polymer complexes are expected to become an efficient oxygen carrier with a sufficient operational lifetime.

For example, the operational lifetime of a picketfence cobaltporphyrin-polymer complex in a solid state is much longer than that of monomeric complexes and the complex in a solution, and it maintains its oxygen-binding ability for over a month at room temperature under an air atmosphere. This enhanced stability of the carriers provides a great advantage for solid membranes.

Oxygen-binding of a cobaltporphyrin-polymer complex is monitored by a reversible change in the UV/vis absorption spectrum. For example, complexation of CoP to an imidazole residue of the poly(vinylimidazole-*co*-octyl methacrylate) (OIm) yielded both an active and homogenous dispersed CoP for oxygen-binding in the solid state.[40] The red color of the transparent CoP-OIm membrane changed and displayed a reversible change in the spectrum from the deoxy form (λ_{max} = 412, 530 nm) to the oxy or oxygen-binding one (λ_{max} = 429, 547 nm) with an isosbestic point at 420, 539 nm, in response to the partial oxygen pressure of the atmosphere (Figure 10 Inset). Such a reversible spectral change is one of crucial evidences that a cobaltporphyrin acts as an effective oxygen carrier from an equilibrium perspective.

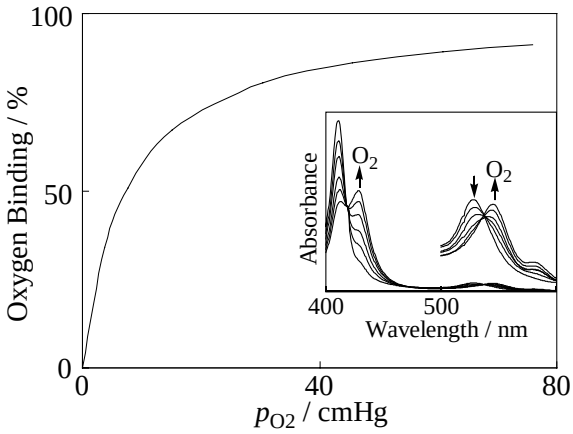

Figure 10. Oxygen-binding equilibrium curve for a CoP-OIm complex in a solid membrane state at 25℃. Insert: UV-visible absorption spectral change of the OIm-OIm complex in response to oxygen partial pressure from 0 to 76 cmHg.

The oxygen-binding equilibrium curve was drawn from the UV/vis absorption spectral change and given in Figure 10. The equilibrium curve obeyed Langmuir isotherm to give the oxygen-binding affinity p_{50} (oxygen partial pressure at which half of the cobaltporphyrin binds with oxygen), as defined by Eq. 7. The oxygen-binding affinity depends on the species of cobaltporphyrin and polymer-ligand, and on the solution (solvent species) or solid state, and also on the temperature. In other words, the oxygen-binding affinity can be controlled with the chemical structures of the cobaltporphyrin and polymer-ligand.

In addition to UV/vis absorption spectroscopy, oxygen-binding to a cobaltporphyrin complex fixed in a solid membrane has also been confirmed with general spectroscopies. For example, by attaching a membrane fragment to the cell window of a simple IR spectrometer, strong IR absorption at 1150 cm^{-1} for $^{16}O_2$ and 1060 cm^{-1} for $^{18}O_2$ attributed to an end-on-type coordination of molecular oxygen to the cobalt ion appeared with an increase in the oxygen partial pressure.[41] Because concentration of the cobalt complex moiety in the polymer domain of the solid membrane is much higher (> 50 mmol l^{-1}) than that of a homogeneously solubilized complex in solution (1 mmol l^{-1}), even a simple spectrophotometer is effective for observing oxygen-binding reactions and ligand-bonding characteristics of complexes.

It is known that metal-coordinated gaseous molecules are photodissociated under flash irradiation, and that their rapid binding reactions can be analyzed, based on the oxygen-binding with a cobaltporphyrin. The photodissociation and binding of oxygen in a solid membrane were observed by improving pulse and laser spectroscopic

techniques.[41] The oxygen-binding rate constants k_{on} and dissociation rate constant k_{off} in Eq. 7 were estimated by second-order kinetics, that is, $k_{on} \sim 10^7\ M^{-1}\ s^{-1}$ and $k_{off} \sim 10^{3\text{-}5}\ s^{-1}$ for the CoP complexes in the membranes.[43] The k_{on} and k_{off} values of the cobaltporphyrins in the solid membrane are similar to those of the complexes in toluene solution. This means that the cobalt complexes are kinetically active for the oxygen-binding even after fixing in dry, solid membranes. From a kinetic point of view, the oxygen-binding reaction of cobaltporphyrins exhibits great promise for the facilitated transport of oxygen through the carrier-mediated membranes and other areas.

The oxygen-binding ability of a variety of cobalt(II) complexes has also been studied.[44-46] An important class of such complexes is represented by the amine cobalt(II) and polyamine chelates in aqueous solution. Their oxygen adducts have been characterized as a μ-peroxo cobalt(III) complex (or $[O_2]$:[Co] = 1:2 type or sandwiched type) as shown in Eq. 11 using the example of the polyethyleneimine-cobalt(II) complex (PEI-Co), where N is the amine group in PEI.

$$2Co(II)N_6 + O_2 \rightleftharpoons N_5Co(III)\text{-}O_2\text{-}Co(III)N_5 + 2N \qquad (11)$$

The pink solution of PEI-Co was immediately changed to a golden brown one upon bubbling oxygen through the solution. The UV-visible absorption spectrum showed a new absorption band at 310 nm, which corresponded to that of the oxygen adduct. An isosbestic point is observed at 275nm. The oxygen-saturated PEI-Co solution was ESR silent, while PEI-Co was paramagnetic in vacuo. This suggested the formation of an oxygen adduct composed of a peroxo (O_2^{2-}) group and a Co(III) ion. Volumetric measurement on the oxygen untake resulted in the stoichiometric formation of an oxygen-Co (1:2) adduct. These results supported a μ-peroxo cobalt(III) complex structure for the oxygen adduct of PEI-Co.

When the oxygen containing brownish PEI-Co solution was allowed to stand under reduced pressure, or when nitrogen was bubbled through the solution, it re-assumed its original pink color gradually. This means that oxygen-binding to PEI-Co is a reversible process and that PEI-Co is able to act as an oxygen carrier in aqueous media at room temperature. [44-45]

1.3 Oxygen Transport through Polymeric Membranes

Oxygen and nitrogen are the top five largest commodity chemicals in the major countries.[47] Oxygen is used for combustion, chemical oxidation, respiratory therapy, refreshment, aquaculture, and wastewater treatment, and nitrogen for purging gases in explosion protection, in food storage, and in manufacture. [48] They are usually produced from air by the cryogenic distillation process and pressure swing adsorption method

(PSA). A polymer membrane process has been considered to be an intriguing candidate as an energy-saving process, especially for the production of oxygen-enriched air or nitrogen-enriched air.[48-49]

Air separation membranes have been developed over the last 30 years based on the selective oxygen permeability of polymeric membranes and later on carrier-mediated transport in liquid and solid membranes. Mixture containing more than 40% (v/v) of oxygen or 95% of nitrogen from air can be obtained through the membrane separation process. For the gas separation, polymers with both high permeability and permselectivity are desirable.[50-51]

1.3.1 Oxygen/nitrogen separation through polymeric membranes

Since oxygen and nitrogen molecules are almost the same in size (oxygen 0.38 nm, nitrogen 0.40 nm), porous membranes for air separation exhibit low selectivity although they provide for very high levels of flux. For example, even in case of a porous membrane with small holes of <1nm, oxygen/nitrogen mixtures can't be separated. In order to overcome this limitation, new dense membranes were designed. [51]

The transport of gases through a dense polymeric membrane is usually described by a solution-diffusion mechanism. The solution-diffusion mechanism is considered to consist of three steps: (1) the adsorption at the upstream boundary, (2) activated diffusion through the membrane, and (3) desorption or evaporation on the other side. The transport is driven by a difference in the thermodynamic activities existing at the upstream and downstream interfaces of the membrane as well as the interacting force working between the polymer membrane material and the permeant molecules. The activity difference causes a concentration difference that leads to diffusion in the direction of decreasing activity.

Air separation through the dense polymeric membranes occurs because of differences in solubility and diffusivity between oxygen and nitrogen, while membrane performance is characterized by permeability and selectivity. Oxygen solubility and diffusivity in and through polymers depend on the nature of the polymers, and are represented by a solubility coefficient (S_{O2}) and a diffusivity coefficient (D_{O2}). Permeability coefficient (P_{O2}) is defined as the product of S_{O2} and D_{O2}, given by Eq 12. Polymers having a little difference between oxygen and nitrogen both in diffusivity and solubility are designed for dense membranes. Typical examples of S_{O2}, D_{O2}, and P_{O2} in polymers are listed in Table 3.[52-53]

$$P_{O2} = D_{O2}S_{O2} \qquad (12)$$

Table 3. Solubility Coefficient (S_{O2}), Diffusion Constant (D_{O2}), and Permeability Coefficient (P_{O2}) of Oxygen in Various Polymer Membranes.

Polymer	*T*g	S_{O2}	D_{O2}	P_{O2}
Poly(1-trimethylsilyl-1-propyne)	> 200	170	45	7700
Polydimethylsiloxane	−123	24	25	610
Poly(cis-1,4-isoprene)	−70	14	1.6	23
Polyethylene	110	6.3	0.46	2.9
Polystyrene	125	7.3	0.11	2.6
Poly(oxymethylene)	191	7.2	0.037	4.2
Poly(vinyl chloride)	324	3.9	0.012	0.045
Poly(ethylene terephthalate)	343	9.2	0.0036	0.03

T_g: ℃; S_{O2}: 10^{-4} cm^3 (STP) cm^{-3} $cmHg^{-1}$; D_{O2}: 10^{-6} cm^2 s^{-1}; P_{O2}: 10^{-10} cm^3 (STP) cm cm^{-2} s^{-1} $cmHg^{-1}$ at 25℃.

The selectivity of a membrane is generally expressed by the ideal separation factor (α), which is defined as the ratio of oxygen permeability coefficient to nitrogen one (Eq. 13).

$$\alpha = P_{O2}/P_{N2} \quad (13)$$

The chemical structure and molecular motion of the polymer determine the separation performance. It was reported that the response of a polymeric material to gas separation is strongly influenced by the polarity and steric characteristics of the polymer and permeate. The size and shape of bulky groups in both the main chain and side chain determine certain fundamental properties like packing density and rigidity, in turn, influence the accessibility. Therefore, it is important to design chemical structure, which increases the difference in *S* and *D* between oxygen and nitrogen without decreasing *S* and *D*.

Polydimethylsiloxane (PDMS) is an important oxygen permselective membrane material because it shows very high P_{O2} (3.5×10^8 cm^3(STP) cm/ cm^2 s cmHg, below the unit of P_{O2} is omitted.). However, PDMS has the low oxygen separation factor (α = 2.0) and possesses no membrane-forming ability. Various modifications have been made to provide PDMS the membrane-forming ability, and to improve the separation factor (α) maintaining the high oxygen permeability. Asakawa et al. prepared a crosslinked polymer from polyvinylphenol (PVP) and PDMS with diethylaminosilyl groups at both ends and showed good membrane-forming ability and high permeability ($P_{O2} = 3.4\times10^8$, α = 2.1).[54] The modified PDMS has been applied to the production of oxygen-enriched air for combustion. Recently Weinkauf et al[55] reported that high oxygen/nitrogen

selectivity (α = 3.1) with a 80% decrease in oxygen permeability was observed after 30 W argon radio frequency (RF)-plasma surface treatments.

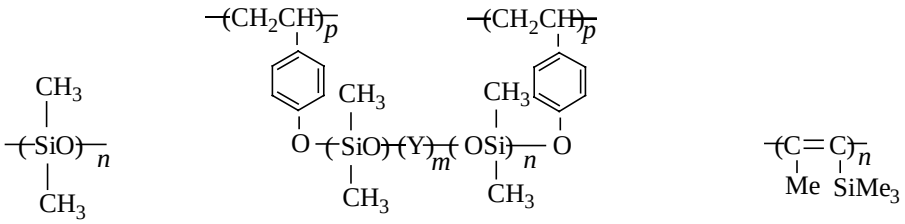

PDMS **PDMS-PVP** **PMSP**

Silicon containing poly(substituted acetylene), for example, poly(1-trimethylsilylpropyne) (PMSP) showed about 10 times higher P_{O2} than that of PDMS, which has the highest P_{O2} (4×10^7) among the commercially available polymers (but the lowest separation factor (α = 1.6)). This is because the intermolecular space is large owing to the stiffness of the main chain, and trimethylsilyl groups with high mobility are located in a space between the main chains where oxygen molecules permeate. Besides that, PMSP has much high content of microvoids than the other polymers in a glassy state.[56] However, the P_{O2} value of this membrane decreased with time and became 1/10 after 10 days at room temperature in vacuo because of change or decrease of the intermolecular space during the physical aging process. When one of the methyl groups of the polymer was replaced by a more bulky substituent, P_{O2} decreased significantly. [57] This indicates the unique properties of PMSP.

The modified polymer, poly[2,4-bis(trimethylsilyl)phenyacetylene], showed a good performance (P_{O2} = 4.73×10^8, α = 2.65). The number and the position of the trimethylsilyl substituent affected P_{O2} and α significantly. The change of P_{O2} upon aging was small. In addition, Oikawa et al.[58] found that polyphenylacetylenes with oligosiloxanes showed a good membrane-forming ability and high P_{O2} value.

In order to improve the separation factor of polymers having high P_{O2} but low α, introducing fluorine-containing groups with high oxygen solubility into these polymers has been reported. For example, when trifluropropyl groups are introduced to the side chains of the block copolymer of poly(tetramethyl-*p*-silphenylenesiloxane), P_{O2} and α simultaneously increased (P_{O2} = 1.94×10^8, α = 2.28). [59] In case of perfluoroalkyl acrylates, monomers having higher contents of fluorine tended to show high values of α.[60]

Although the polymer membranes having both high permeability and permselectivity are desirable, permeability through a polymer membrane correlates inversely with the permselectivity of oxygen relative to nitrogen. Figure 11 is a plot of

oxygen permselectivity (or oxygen separation factor, $\alpha = P_{O2}/P_{N2}$) versus logarithmic oxygen permeability coefficient (P_{O2}) of commercially available polymers. In other words, P_{O2} increases with a decrease in α, i.e. a trade-off relationship and an upper boundary line are present. [61]

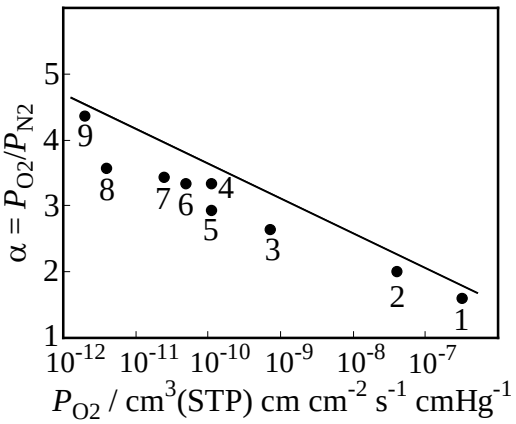

1 poly(1-trimethylsilylpropyne)
2 polydimethylsiloxane
3 cellulose acetate
4 polyethylene
5 polypropylene
6 polycarbonate
7 poly(vinyl chloride)
8 nylon 6
9 poly(ethylene terephthalate)

Figure 11. A plot of oxygen/nitrogen selectivity (α) versus oxygen permeability coefficient (P_{O2}) of commercially available polymers.

1.3.2 Facilitated oxygen transport through cobaltporphyrin membranes

The application of polymer membranes in gas separation has, however, been limited by the difficulty of preparing membranes with the desirable combination of high selectivity, which yields high product purity and low operating costs, and high permeability, which reduces membrane area and capital cost.[46] To improve both the selectivity and permeability, a solid membrane using the concept of facilitated transport mediated with a fixed carrier has thus been considered to be a very promising alternative. [62]

Facilitated oxygen transport through the membrane containing carrier molecules has been investigated since the first paper of Scholander [63] and the second paper of Wittenberg [64]. They showed that hemoglobin (Hb) and myoglobin could accelerate the transport of oxygen across water films and arose the interest in the synthesis of oxygen carriers. The first to apply synthetic oxygen carriers was Basset in 1970,[65] who used bis(histidine)cobalt (II) as an oxygen carrier in an aqueous medium. The best results gave an approximate doubling of the oxygen flux compared to water and a selectivity of 3.5.

Although the liquid membranes holding the metal complexes provided an elegant method for improving both the selectivity and flux, there remained the unresolved issues, such as evaporation loss of liquid, chemical instability of carrier, limited carrier

solubility in the liquid membranes. To overcome these problems, over the past years researchers have been attempting to replace the liquid membrane with a solid one in which the carrier is embedded.[52]

Figure 12 schematically represents the facilitated transport of oxygen via a fixed carrier in a solid membrane. The fixed carrier picks up oxygen specifically from air at the upstream interface. This specific and reversible oxygen-binding reaction establishes a steep gradient in the oxygen concentration across the membrane from the upstream side to the downstream side, in response to which the oxygen taken up in the membrane is transferred via the fixed carrier to the downstream side. At the membrane-downstream interface, the carrier releases oxygen, thereby resulting in facilitated transport. That is, the driving force to yield the facilitated oxygen transport is the concentration gradient of oxygen in the membrane or selectively enhanced solubility of oxygen. The binding and releasing reactions occur repeatedly across the membrane. Thus, the oxygen solubility, and binding-releasing reaction rates between the carrier and oxygen are major parameters in determining the transport properties. In order to enhance the facilitated transport of oxygen in the membrane, the carrier has to possess both a strong oxygen-binding affinity and fast oxygen-dissociation kinetics.

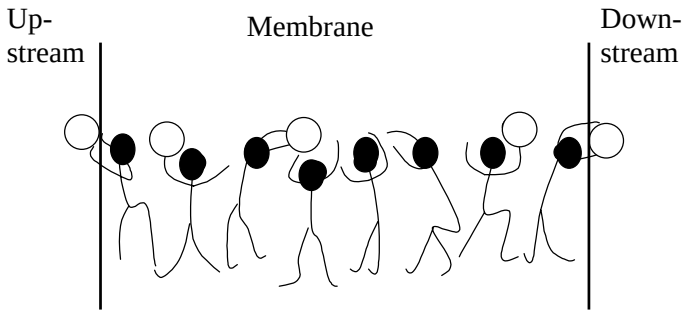

Figure 12. Facilitated oxygen transport via a fixed site carrier of polymer-metal complex in a solid membrane.

Fixed carrier membranes in a solid state provide the following advantages over liquid membranes for air separation: (1) higher stability of the carrier, (2) higher mechanical strength, (3) no liquid loss, (4) possibility of incorporating a larger amount of the carrier in the matrix, and (5) flexibility as regard controlling the membrane thickness to enhance the flux.

The facilitated oxygen transport through a solid polymer complex membrane was first achieved by incorporating a picketfence cobaltporphyrin characterized with both rapid kinetics and a strong affinity for oxygen-binding as a chemically selective oxygen-binding site. [2,52] The oxygen permeability coefficient P_{O2} for the membrane is shown in Figure 13. P_{O2} is larger than P_{N2} and steeply increases with a decrease in the

oxygen upstream pressure (p_{O2}). On the other hand, P_{N2} is small and independent of the nitrogen upstream pressure (p_{N2}), because the fixed cobaltporphyrin does not interact with nitrogen. P_{O2} is also small and independent of p_{O2} for the control membrane composed of an inert Co(III) complex, which does not interact with oxygen. That is, the active cobaltporphyrin fixed in the polymer membrane facilitates oxygen transport and enhances the oxygen permeation, represented by the shadowed area in Figure 13. P_{O2} also increases with the cobaltporphyrin concentration in the polymer membrane. The oxygen/nitrogen selectivity (P_{O2}/P_{N2}) was 3.2, 4.4, and 7.5 for a membrane containing 0, 2.5, and 4.5 wt% picket-fence cobaltporphyrin, respectively. This result indicates both a high selectivity and permeability for a solid-state polymer membrane containing an oxygen carrier.

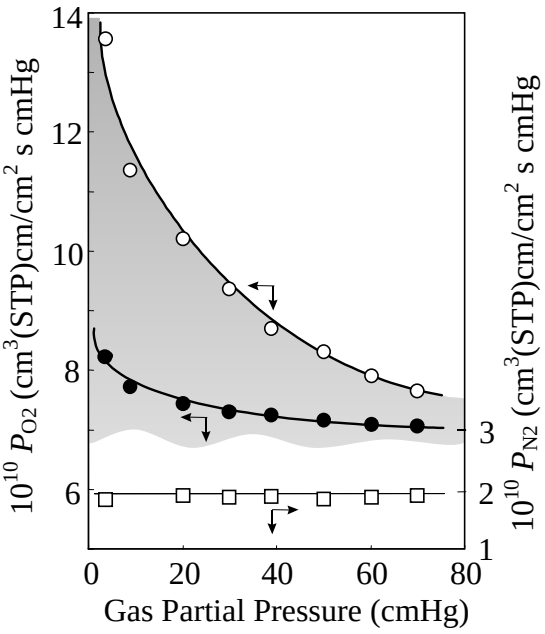

Figure 13. Oxygen and nitrogen permeability coefficients (P_{O2} and P_{N2}) for the cobaltporphyrin-polymer complex membrane. The cobaltporphyrin concentration in the OIm membrane: ○: 4.5%; ●: 2.5%; and □: nitrogen for 4.5% at 30℃.

A few mathematical models have been developed to analyze the facilitation phenomena in a fixed carrier membrane.[66-70] The dual transport model that was originally developed to interpret the transport behavior of gases or vapors in glassy polymers has been commonly employed, because it is conceptually analogous to the mass transport in a facilitated transport membrane with fixed carriers. [66,69]

Figure. 14 is a schematic representation of the oxygen permeability in a cobaltporphyrin-polymer membrane governed by two modes.[52] That is, the oxygen permeation is equal to the sum of the first term that represents the physical permeation

mode and the second term that represents the carrier-mediated permeation model. For the physical mode (upper permeation route in Figure 14), oxygen physically dissolves in the polymer membrane, according to Henry's law, then the dissolved oxygen diffuses physically. For the carrier-mediated mode (the lower permeation route in Figure 14), oxygen is specifically and chemically taken up by the cobaltporphyrin fixed in the membrane and hops from one cobaltporphyrin to another by repeating a binding and releasing reaction to and from the cobaltporphyrin. The oxygen transport is thus accelerated by this carrier-mediated mode in addition to the physical mode.

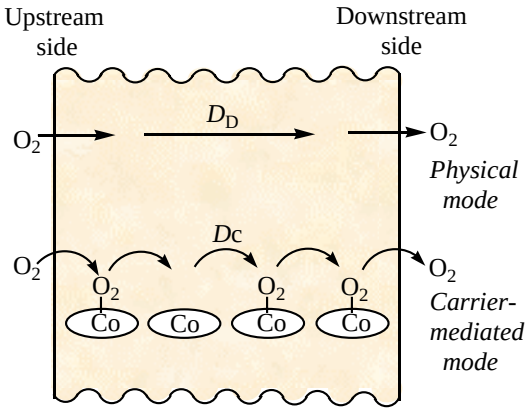

Figure 14. Dual-mode oxygen transport in the solid-state polymer membrane containing cobaltporphyrin as a fixed carrier of oxygen.

The dual-mode-transport model is mathematically described in Eq. 14. Here, D_D is the physical diffusion coefficient of oxygen in the membrane, and D_C is the postulated diffusion coefficient of oxygen that hops via the fixed cobaltporphyrin carrier. k_D and C_C correspond to the physical solubility coefficient of oxygen and the concentration of active cobaltporphyrin incorporated in the membrane. K is the oxygen-binding equilibrium constant of the cobaltporphyrin fixed in the membrane.

$$P_{O2} = k_D D_D + \frac{C_C K D_C}{1 + K p_{O2}} \qquad (14)$$

The effect of p_{O2} on P_{O2} in Figure 13 was analyzed using Eq. 14, that is, P_{O2} was plotted versus $1/(1+Kp_{O2})$.[2,71] The plotted showed a linear relationship to yield the diffusion coefficients, $D_D = 10^{-6}$ cm^2 s^{-1}, and $D_D = 10^{-8}$ cm^2 s^{-1}. The D_D value agreed with the previously reported diffusion coefficient of oxygen in an amorphous polymer with a similar T_g. D_C is smaller than D_D, because the chemical binding reaction of oxygen with the cobaltporphyrin suppresses the oxygen diffusivity. D_C increased with C_C or the active cobaltporphyrin concentration in the membrane. D_C also depended on the cobaltporphyrin species or the oxygen-binding properties of cobaltporphyrins. D_C

has been found to be inversely proportional to the average distance between the cobaltporphyrin sites, [72] thereby supporting the postulation that D_C represents the oxygen hopping diffusivity via the fixed cobaltporphyrin carriers, as illustrated in Figure 14. The multiplication of the increases in both C_C and D_C significantly enhances the second (chemical) term in Eq. 14. As a result, both P_{O2} and the oxygen/nitrogen permselectivity increase with the active cobaltporphyrin concentration in the membranes, which can be clearly ascribed to the facilitated oxygen transport by the fixed cobaltporphyrin carriers.

Recently, Merkel et al reported that physical dispersion of nanoporous, nanoscale, fumed silica particles in glassy amorphous poly(4-methyl-2-pentyne) simultaneously and surprisingly enhances both membrane permeability and selectivity for large organic molecules over small permeate gases. These highly unusual enhancements, in contrast to results obtained in conventional filled polymer systems, reflect fumed silica-induced discruption of polymer chain packing and an accompanying subtle increase in the size of free volume elements through which molecular transport occurs.[73]

1.4 Oxygen Electrode and its Applications

Oxygen electrode is typically applied as cathode for air batteries and fuel cells,[74-76] and its design with improved performance is one of the important goals in electrochemical oxygen technology.

1.4.1 Metal/air batterers and fuel cells

Metal/air batteries and fuel cells are electrochemical devices that produce electricity through clean chemical reactions rather than environmental detrimental processes like combustion. They have been attracted particular attentions due to their numerous benefits, such as lower emissions, high efficiency even at part load and possibly lower requirements for maintenance.[77]

Metal/air batteries Metal/air batteries contain metal (negative) anodes and oxygen (positive) cathodes, with the oxygen usually obtained from air. These batteries are classified according to the type of metal anodes since oxygen is a common feature. Table 4 summarizes the electrochemical features for various metals (e. g., Al, Fe, Li, Zn, Mg, Cd, Pd) in metal/air batteries containing alkaline electrolytes.[78] Because the supply of air is virtually inexhaustible, the oxygen electrode in metal/air batteries can, in principle, function indefinitely, and its capacity can be considered infinite. In addition, the advantage of metal/air batteries over many other conventional batteries is their potentially high specific energy (Wh/kg), which is a result of the low equivalent weight of oxygen (8 g/equivalent) compared to most oxidants that react at the cathode. A

zinc/air battery is shown schematically in Figure 15. [79]

The origin of metal/air batteries can probably be traced back to about 1868 when Leclanche observed that the performance of the batteries improved when MnO_2/carbon electrodes were only partially immersed in the electrolyte. The enhanced performance is attributed to the depolarizing action of oxygen at the porous carbon electrode. In 1879, Maiche omitted MnO_2 from the electrode and added Pt to the carbon powder to demonstrate the concept of a zinc/air battery. Heise and Schumacher are credited with the development in 1932 of the modern version of the zinc/air battery. [80]

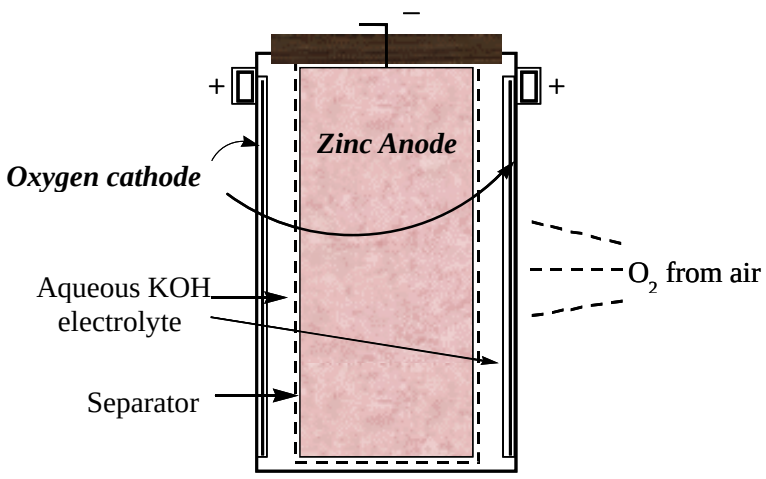

Figure 15. Schematic diagram of a zinc/air battery.

Table 4. Summary of Metal/Air Batteries with Alkaline Electrolytes.

Metal/ air cell	Anode reaction	Anode potential [a] /V	Metal equiv. /Ah g^{-1}	Cell voltage[b] /V		Specific energy /kWh kg^{-1}	
				T[c]	O[d]	Metal	Cell
Zn/air	$Zn + 2OH^- \rightarrow Zn(OH)_2 + 2e^-$	-1.25	0.82	1.65	1.0-1.2	1.3	0.9
Fe/air	$Fe + 2OH^- \rightarrow Fe(OH)_2 + 2e^-$	-0.88	0.96	1.28	1.0	1.2[e]	0.8
Al/air	$Al + 3OH^- \rightarrow Al(OH)_3 + 3e^-$	-2.30	2.98	2.70	1.2-1.6	8.1	2.8
Li/air	$Li + OH^- \rightarrow LiOH + e^-$	-3.05	3.86	3.45	2.4	13.3	3.9
Mg/air	$Mg + 2OH^- \rightarrow Mg(OH)_2 + 2e^-$	-2.69	2.20	3.09	1.2-1.4	8	2.8
Ca/air	$Ca + 2OH^- \rightarrow Ca(OH)_2 + 2e^-$	-3.01	1.34	3.42	2.0	4.6	2.5

[a] The anode potential was vs. the standard hydrogen electrode (SHE). [b] When coupled with an oxygen cathode. [c] Theoretic condition. [d] Operating condition. [e] 1.8 kWh/kg for Fe^{3+}.

The major development effort to date has focused on metal/air batteries containing alkaline electrolytes, with a small effort on batteries containing saline electrolyte. The electrochemical reactions involving oxygen are kinetically more favorable in alkaline electrolyte than those in acidic and neutral electrolytes, consequently, the high-pH electrolytes are of more interest for practical metal/air batteries.

The metal such as Li, Al, Mg, and Ca in alkaline electrolytes can, in theory, provide high electrode potentials. However, these metals cannot be electrodeposited from aqueous electrolytes; consequently, they are practical only in primary batteries. On the other hand, Zn and Fe can be electrodeposited from aqueous electrolytes, thus making them possible candidates in secondary (electrically recharged) metal/air batteries. For example, the high theoretical (1150 Wh kg^{-1}) as well as practical specific energy (60-150 Wh kg^{-1}) are major advantages of the secondary zinc/oxygen battery. The low cost and low toxicity of the materials involved are also important factor.[81]

Fuel cells The principle of fuel cell was first discovered in 1839 by Sir William R. Grove, who used hydrogen and oxygen as fuels catalyzed at platinum. [82] The basic elements of a typical fuel cell consist of an electrolyte phase in intimate contact with an anode and a cathode. The fuel and oxidant gases flow past the backside of the anode and cathode, respectively, and react electrochemically in the region of the three-phase boundary established at the gas/electrolyte/electrode interface. A typical fuel cell is shown schematically in Figure 16. In the process, a hydrogen ion travels through the electrolyte and the electron released by the ionization of the hydrogen atom travel through a circuit and provides power. The hydrogen ions and electrons are hence combined with oxygen at the cathode and form water in acidic solutions. [83]

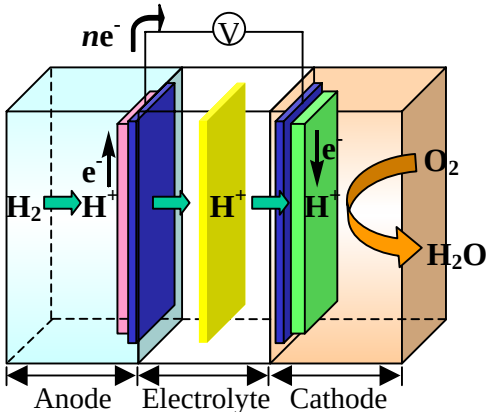

Figure 16. Schematic diagram of a typical example of fuel cells.

On the basis of the electrolyte employed, there are five types of fuel cells. They are polymer electrolyte fuel cells (PEFC), alkaline fuel cells (AFC), phosphoric acid fuel cells (PAFC), molten carbonate fuel cells (MCFC), and solid oxide fuel cells (SOFC). Table 5 summarized the features of the four main types of fuel cells.[84] As the operating temperature of a fuel cell increases, the oxygen electrode kinetics improves and electrocatalysis becomes less important. Instead, technical problems related to material stability and component fabrication become more important.

Table 5. Types of Fuel Cells and their Features.

Features	Fuel cell type			
Name	PEFC	PAFC	MCFC	SOFC
Electrolyte	Ion exchange membrane	Phosphoric acid	Alkaline carbonate mixture	Yttria-stabilized zirconia
Temperature /℃	70-90	180-220	650-700	800-1000
Charge Carrier	H^+	H^+	CO_3^{2-}	O^{2-}
Electrolyte state	Solid	Immobilized liquid	Immobilized liquid	Solid
Cell hardware	Carbon- or metal-based	Graphite-based	Stainless steel	Ceramic
Catalyst, anode	Platinum (Pt)	Platinum (Pt)	Nickel (Ni)	Nickel (Ni)
Fuels for cell	H_2	H_2	Reformate or CO/H_2	Reformate or CO/H_2 or CH_4
Reforming	External or direct MeOH	External	External or internal	External or internal, or direct CH_4
Feed for fuel processor	MeOH, natural gas, LPG, gasoline, diesel, jet fuel	Natural gas, MeOH, gasoline, diesel, jet fuel	Gas from coal or biomass, natural gas, gasoline, diesel, jet fuel	Gas from coal or biomass, natural gas, gasoline, diesel, jet fuel
Oxidant for cell	O_2/air	O_2/air	CO_2/O_2/air	O_2/air
Co-generation heat	None	Low quality	High	High
Cell efficiency /% LHV	40-50	40-50	50-60	50-60

Table 6. Typical Electrochemical Reactions in Fuel Cells.

Fuel cell	Anode reaction	Cathode reaction
PEFC	$H_2 \rightarrow 2H^+ + 2e^-$	$O_2 + 4H^+ + 4e^- \rightarrow 2H_2O$
AFC	$H_2 + 2OH^- \rightarrow 2H_2O + 2e^-$	$O_2 + 2H_2O + 4e^- \rightarrow 4OH^-$
PAFC	$H_2 \rightarrow 2H^+ + 2e^-$	$O_2 + 4H^+ + 4e^- \rightarrow 2H_2O$
MCFC	$H_2 + CO_3^= \rightarrow H_2O + CO_2 + 2e^-$	$O_2 + 2CO_2 + 4e^- \rightarrow 2CO_3^=$
SOFC	$H_2 + O_3^= \rightarrow H_2O + 2e^-$	$O_2 + 4e^- \rightarrow 2O^=$

The electrochemical reactions occurring in the five major types of fuel cells are listed in Table 6. With the exception of MCFC, the reactions at the anode and cathode generally involve only the gaseous hydrogen, and nitrogen, respectively.

The amount of current available to the external circuit depends on the chemical activity and amount of the substances supplied as fuels and the loss of power inside the

fuel cell stack. The current densities obtained at smooth electrodes are usually in the range of a few mA/cm^2 or less because of rate-limiting processes such as mass transport of reactant to the electrode surface. In porous electrodes containing high interfacial areas, current densities of the order of about 1000 mA/cm^2 are achievable.[80]

1.4.2 Oxygen reduction at the cathode

The cathodic reduction of oxygen is one of the most widely studied electrochemical reactions. The kinetics and mechanism for the oxygen reduction are functions of many factors, including the type of cathode material (e.g., electrocatalyst) and electrolyte.

Reduction pathway of oxygen Depending on the electrode material, oxygen reduction may involve either 4-electron pathway or peroxide pathway or both.[80,85]

Direct 4-Electron Pathway

In alkaline solutions:

$$O_2 + 2H_2O + 4\,e^- \rightarrow 4OH^- \qquad E_0 = 0.401 \text{ V vs. SHE} \qquad (15)$$

In acidic solutions:

$$O_2 + 4H^+ + 4\,e^- \rightarrow 2H_2O \qquad E_0 = 1.229 \text{ V vs. SHE} \qquad (16)$$

Peroxide Pathway

In alkaline solutions:

$$O_2 + H_2O + 2\,e^- \rightarrow HO_2^- + OH^- \qquad E_0 = -0.065 \text{ V vs. SHE} \qquad (17)$$

following by either the reduction of peroxide

$$HO_2^- + H_2O + 2\,e^- \rightarrow 3OH^- \qquad E_0 = 0.867 \text{ V vs. SHE} \qquad (18)$$

or the decomposition of peroxide

$$2HO_2^- \rightarrow 2OH^- + O_2 \qquad (19)$$

In acidic solutions:

$$O_2 + 2H^+ + 2\,e^- \rightarrow H_2O_2 \qquad E_0 = 0.67 \text{ V vs. SHE} \qquad (20)$$

following by either the reduction of peroxide

$$H_2O_2 + 2H^+ + 2\,e^- \rightarrow 2H_2O \qquad E_0 = 1.77 \text{ V vs. SHE} \qquad (21)$$

or the decomposition of peroxide

$$2H_2O_2 \rightarrow 2H_2O + O_2 \qquad (22)$$

The direct 4-electron pathway involves a large number of reaction intermediates

and rate-determining steps in which oxygen is reduced to OH^- or water. The reduction steps may involve an absorbed peroxide intermediate, but this species does not lead to peroxide in the solution phase. On the other hand, the peroxide pathway involves peroxide species that are present in solution. If these species decompose in solution, the resulting oxygen is recycled via reaction (17) or (20) (depending on pH), and the overall reaction is the 4-electron pathway.

4-Electron transfer is desirable for the practical use of oxygen electrode in air batteries and fuel cells. It was found that 4-electron pathway appears to be predominant on noble-metal electrocatalysts (e.g., Pt, Pd, Ag), metal oxide (e.g., perovskites, pyrochlores), and some transition-metal macrocyclics (e.g., iron tetrasulfonated phthaocyanine, dicobalt face-to-face diporphyrin complexes on graphite) that are N_4 chelates. While the peroxide pathway is predominant on graphite, most carbons, most oxide-covered metals (e.g., Ni, Co), most transition-metal oxides (e.g., NiO, spinels), and some transition-metal macrocycles (e.g., cobalt tetrasulfonated phthalocyanine, cobalt tetramethoxyphenyl porphyrin).[80]

Potential and current The reduction potential and current of oxygen are important electrochemical parameters. The potential is related to the free energy of a reversible electrochemical reaction, while the transport-limited electrochemical reduction rates or current are determined by the solubility and diffusivity of oxygen.

It is the change in Gibbs free energy that is converted to electrical energy. The relationship between the free energy ($\triangle G^\circ$) of the overall chemical reaction and the standard cell potential for thermodynamic equilibrium in the absence of a current flow (E°_{cell}) is shown in Eq. 23, where n is the total number of electrons transferred in the reaction, F is Faraday's constant.[86]

$$\triangle G^\circ = -nF\,E^\circ_{cell} \qquad (23)$$

Regarding a fuel cell that produces the electromotive force by electrochemical reactions when supplied on the anode with hydrogen and on the cathode with oxygen in the acidic electrolytes, the cell reaction is represented in Eq. 24, the equilibrium cell potential is 1.23V corresponding to the $\triangle G$ of –237 kJ/mol for the overall reaction at standard conditions (25℃).

$$O_2 + 2H_2 \rightarrow 2H_2O \qquad (24)$$

The current i which affords an instantaneous measurement of the rate of the electrochemical reaction are determined by the active surface area of the electrode and the reaction rate are represented by Eq. 25, where n is the number of electrons

transferred in the interfacial reaction process, *A* is the surface area of the electrode interface, *r* is the instantaneous reaction rate.

$$i = nFAr \tag{25}$$

The electrode potential can be considered as an adjustable driving force for the electrochemical reaction. For a process involving four-electron transfer of oxygen reduction in acidic electrolyte (Eq. 16), the thermodynamic potential (*E*) is given by the well known Nernst equation (Eq. 26), where E^0 is theoretical potential calculated from the free energy; α_{O2}, α_{H+} and α_{H2O} are the activity coefficients of oxygen, proton and water.

$$E = E^0 + \frac{RT}{4F}\ln\frac{\alpha_{O_2}\alpha_{H^+}{}^4}{\alpha_{H_2O}{}^2} \tag{26}$$

To avoid the complications associated with the use of thermodynamic activities and activity coefficients, activities are replaced by concentrations. In this case, the standard potential is replaced by the formal potential, $E^{0'}$, which is usually dependent on medium conditions since it includes the activity coefficients. Therefore, a more practical version of the Nernst equation is represented by Eq. 27.

$$E = E^{0'} + \frac{2.303RT}{4F}\log\frac{[O_2][H^+]^4}{[H_2O]^2} \tag{27}$$

Kinetics of oxygen reduction Oxygen reduction is a heterogeneous process that takes place at the interface between the electrode and the electrolyte. Therefore, the overall reduction rate or current depends on the rates of two distinct processes: the interfacial electron transfer at the electrode and the transport of oxygen from the solution to the electrode surface. The slower one of the two processes determines the overall current. Figure 17 illustrates this situation clearly. The curve is composed of three distinctive regions. In the first region, there is no significant current flow because of the potential is not sufficient to drive electrochemical reaction. In the second region, the current increases with the potential. In this region the electron transfer process controls the current level and mass transport is still sufficiently fast. In the third region the current reaches a constant or limiting value independent from the potential. This is due to limitations imposed by the finite rate of mass transport. Therefore, the magnitude of the solubility and diffusivity of oxygen plays a significant role in the limiting current density (i_l) for oxygen reduction, as is evident in the equation for Fick's first law (Eq. 28), where *D* is the oxygen diffusion coefficient, *C* is the solubility of oxygen in the bulk electrolyte, and δ is the thickness of the mass-transfer boundary layer. It is apparent

that the limiting current density increases with an increase in the solubility and diffusion coefficient of oxygen, and with a decrease in the boundary-layer thickness.[80]

$$\frac{i_l}{nF} = \frac{DC}{\delta} \tag{28}$$

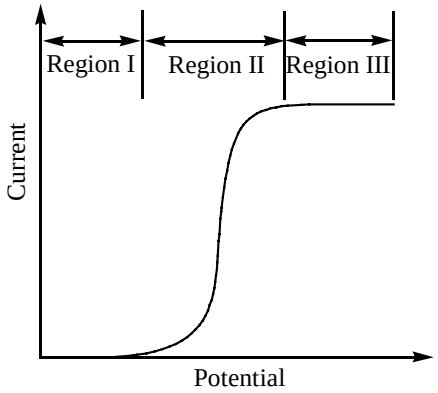

Figure 17. A typical current-potential curve.

The empirical Tafel equation (Eq. 29) establishes a mathematical relation between the current and the overpotential η (difference between the applied potential and the corresponding equilibrium potential for the electrode), where *a*, and *b* are constant values of the system.

$$\eta = a + b \log i \tag{29}$$

$$r = kC_{O_2}(t) = \frac{i_C}{nFA} \tag{30}$$

For the oxygen reduction reaction in an acidic solution, we deduce Eq. 30 from Eq. 25, in which *k* is the rate constant for the reduction reaction, $C_{O2}(t)$ is the oxygen concentration at the electrode surface at time *t*, i_C is the cathodic current. The heterogeneous character for the process is manifested by the fact that the reaction rate is directly proportional to the oxygen concentration.

A distinguishing feature of electrochemistry is that the reaction rates depend on the applied electrode potential. Butler-Volmer formulation shows the phenomena (Eq. 31),

$$k = k^0 e^{-\alpha nF(E-E^{0'})/RT} \tag{31}$$

where k^0 is the standard rate constant and α is the so-called transfer coefficient.[87] From Eq. 31, we know that the reaction rate (*k*) is zero at equilibrium ($E = E^{0'}$). [88]

The inherent slow kinetics of the electrochemical reactions involving oxygen, especially in acidic and neutral electrolytes, have prompted extensive studies to enhance

the rate of electron transfer, which have spawned a number of electrocatalysts.[80] A major breakthrough in oxygen electrode was the development of various alternatives as a replacement for platinum, e.g. manganese dioxide, cobalt tetramethoxy porphyrin, perovskite-type oxides etc. [89-90]

The cathodic reduction of oxygen occurs at practical current densities with high polarization, even with the most active electrocatalysts and with electrodes of optimized structures. Examples of typical cathode polarizations at ～200mA/cm^2 in various fuel cells are presented in Table 8. At the higher operation temperature of MCFC, activation polarization at the oxygen cathode is reduced considerably, as is also evident in AFC operating at 200℃ with oxygen. On the other hand, the fuel cells with aqueous electrolytes exhibit high cathode polarization. Some measures have been taken to lower the polarization of oxygen electrode, such as utilizing improved electrocatalysts and optimizing the porous electrode structure. Platinum-based materials are the optimum electrolysts for oxygen reduction in acidic electrolytes. In alkaline electrolytes, a wider selection of potential electrocatalysts is available, and material that do not contain noble metals are extremely promising.

Table 8. Activation Polarization[a] for Oxygen Cathodes in Various Fuel Cells.

Fuel cell	Anode	Cathode	Temperature /℃	Polarization /V
AFC	Pt	Pt	65	0.25-0.35
PEFC	Pt	Pt	100	0.25
PAFC	Pt	Pt	～190	0.4
AFC	Ni	NiO	200	0.1[b]
MCFC	Ni	NiO	650	<0.1

[a] ～200mA/cm^2 in air

[b] Pure oxygen at cathode instead of air

1.4.3 Combination of the electrode with an oxygen enriching system

The physicochemical properties of oxygen, such as its diffusivity and solubility, have a significant influence on the cathodic reaction in air batteries and fuel cells. According to Eq. 27 and 30, the potential and current of oxygen reduction increase with an increase in the oxygen concentration near at the interface of the cathode.

In traditional oxygen electrodes, sufficient porosity with extended reaction zones in the electrode/liquid/gas interface is used to facilitate transport of oxygen from the air to the oxygen electrode (the so-called gas-diffusion electrode).[91] Sometimes the maximum discharge current that can be drawn from Zn/air cells depends on the number of air holes in the cover, and on the cell orientation. But restricting gas diffusion into small metal/air cells by varying the size and number of air holes is a difficult task, especially

in cells that are required to operate for several years at currents of a few microamperes. Therefore, the discharging current is often limited by the transport of oxygen. [80,92-94]

The oxygen concentration near a cathode is proportional to the oxygen partial pressure and the oxygen concentration in the atmosphere. It means that an increase in the oxygen partial pressure or oxygen concentration in the atmosphere or both results in the increase of the potential and current of the cathode. A widely adopted conventional practice has therefore been to incorporate a compressor into the fuel-cells system and to supply the fuel cells with air compressed by the compressor. The aim of this practice is to raise the total pressure of the air and thus increase the electromotive force of the fuel cells. [91]

The higher oxygen concentration can also be achieved by raising the oxygen concentration of the supplied gas. Therefore, concerning the oxygen-consuming cathodic reaction, the development of oxygen permselective polymer membranes with good fluxes is needed.[95]

Sanyama et al.[96] proposed a method that supplied an oxygen electrode with oxygen selectively separated from air by use of an oxygen permeable membrane. Kaneko et al. [97] proposed a method for increasing the oxygen concentration of the gas supplied to a fuel cell by removing nitrogen from air by use of a nitrogen separator installed in the fuel-cells apparatus. By use of these methods, the oxygen concentration supplied to the oxygen electrode can be increased, therefore, to enhance the power generating performance of the fuel cell.

To secure of an adequate gas flow by this method, the amount of air processed has to be increased by using a large area permeable membrane and/or making the pressure differential between the opposite sides of the permeable membrane great. However, the size of the overall device increases in proportion to the area of the membrane and energy consumption rises in proportion to the pressure differential. The method using an oxygen permeable membrane is therefore difficult to adopt for supply of oxygen to fuel cells for powering an electric vehicle.

Motomatsu et al [98] suggested a specific method that supplied an oxygen electrode with oxygen-enriched air by the pressure swing absorption method (PSA). The PSA method consists in passing air removed of water vapor and carbon dioxide through a molecular sieve made of zeolite or the like to cause mainly the nitrogen to be absorbed by the zeolite and thereby obtain a gas of high oxygen partial pressure. The PSA method can provide a gas having very high oxygen partial pressure (oxygen concentration of 90% or more). However, the PSA method also has disadvantages,. One is that the large amount of zeolite or other adsorbent needed increases the size of the apparatus. Another

is that a large amount of electric power is needed to drive the device. These drawbacks make the PSA method difficult to apply practically in the fuel cells.

Nitta et al.[99] equipped a fuel cell system with an oxygen enrichment device wherein fuel cells power generating efficiency is enhanced by increasing the oxygen concentration of the gas. The oxygen enrichment unit is a magnetic oxygen enrichment device that effects oxygen enrichment utilizing the fact that the oxygen molecule is paramagnetic.

Until now there is no report that polymer-metal complexes having a reversible oxygen-binding ability are employed for the modification of an electrode surface with a view to accumulate oxygen from the electrolyte solution and allow the efficient electroreduction of oxygen.

References

1. Jones R.D., Summerville D. A., Basolo F. *Chem. Rev.* **1979**, *79*, 139.
2. Nishide, H., Tsuchida E. *Macromolecules-Matal Complexes*, Springer-Verlag: Berlin, **1996**.
3. Marvel C. S., Tarkoy N. *J. Am. Chem. Soc.* **1957**, *79*, 6000.
4. Goodwin H. A., Bailar J. C. *J. Am. Chem. Soc.* **1961**, *83*, 2467.
5. Hartley F. R. *Supported Metal Complexes. A New Generation of Catalysts*, Reidel Pub. Co., Dordrecht, **1985**.
6. Pomogailo A. D. *Catalysis by Polymer–Immobilized Metal Complex*, Gordon and Breach Publ., Amsterdam, **1998**.
7. Tsuchida E., Nishide H. *Topics Curr. Chem.*, **1986,** *132*, 64.
8. Kaneko M., Yamada A. *Adv. Polym. Sci.* **1984**, *55*, 1.
9. Godovski D. Y. *Adv. Polym. Sci.*, **1995**, *119*, 79.
10. Pomogailo A. D. *Russ. Chem. Rev.*, **2000**, *69*, 53.
11. Biswas M., Mukherjee A. *Adv. Polym. Sci.*, **1994**, *115*, 89.
12. Tsuchida E., Nishide H. *Adv. Polym. Sci.* **1977**, *24*, 1.
13. Kaliyappan T., Kannan P. *Prog. Polym. Sci.*, **2000**, *25*, 343.
14. Belfiore L. A., Pires A., Wang Y., Graham H., Ueda E. *Macromolecules*, **1992**, *25*, 1411.
15. Belfiore L. A., Indra E., Das P. *Macromol. Symp.*, **1997**, *114*, 35.
16. McCurdie M., Belfiore L. A. *J. Polym. Sci., Part B: Polym. Phys.*, **1999**, *37*, 301.
17. Nishide H., Chen X.-S, and Tsuchida E. *Functional Monomers and Polymers*, Takemoto K., Ottenbrite R. M, Kamachi M. Ed., Marcel Dekker: New York, Chapter 6, pp173, **1997**.

18. Tsuchida E., Nishide H. *ACS Symp Ser*, **1980**, *121*, 147.
19. Kaliyappan T., Kannan P. *J. Polym, Sci. A: Polym. Chem.*, **1996**, *34*, 3551.
20. Lamba J., Fraser C. *J. Am. Chem. Soc.*, **1997**, *119*, 1801.
21. Nguyen P., Gomez-Elipe P., Manners I. *Chem. Rev.*, **1999**, *99*, 1515.
22. Anson F. C., Shi C., Steiger B. *Acc. Chem. Res.*, **1997**, *30*, 437.
23. Shi C., Anson F. C. *Inorg. Chem.*, **1992**, *31*, 5078.
24. Wright P. V. *Br. Polym. J.*, **1975**, *7*, 319.
25. Angell C. A., Lin C., Sanchez E. *Nature*, **1993**, *362*, 137.
26. Watanabe M., Yamada S., Sanui K., Ogata N. *J. Chem. Soc. Chem. Commun.*, **1993**, 929.
27. Murata K., Izuchi S., Yoshihisa Y. *Electrochimica Acta*, **2000**, *45*, 1501.
28. Mark T. J. *Angew Chem.*, **1990**, *102*, 886.
29. Ramraij R., Kaneko M. *Adv. Polym. Sci.*, **1995**, *123*, 216.
30. Kaneko M., Yamada A. *Adv. Polym. Sci.*, **1984**, *55*, 1.
31. Vernon F., Shah T. *React. Polym.*, **1983**, *1*, 301.
32. Collman J. P. *Acc. Chem. Res.* **1977**, *10*, 265.
33. Figoli A., Sager W. F. C., Mulder M. H. V. *J. Membr. Sci.*, **2001**, *181*, 97.
34. Momenteau M., Reed C.A. *Chem. Review*, **1994**, 94, 659.
35. Kadishi K. M., Smith K. M., Guilard R. Ed. *The Porphyrin Handbook*, Vol. 4, Academic Press, Oxford, **1996.**
36. Tsuchida E., Nishide H. *Adv. Polymer Sci.*, **1997**, *24*, 1.
37. Suzuki Y., Nishide H., Tsuchida E. *Macromolecules*, **2000**, *33*, 2530.
38. Dolphin D. Ed. *The Porphyrins*, Vol. V, Academic Press, New York, **1978**.
39. Antonelli M. L., Bucci R., Carunchi V., Cernia E. *J. Polym. Sci. Polym Chem Ed*, **1980**, *18*, 179.
40. Shinihara H., Arai T., and Nishide H. *Macromol. Symp.*, **2002**, *186*, 135.
41. Nishide H., Tsuchida E. *Macromolecular Complexes*, Tsuchida E. Ed. VCH Publishers, New York, Chapter 6, **1991.**
42. Tsuchida E., Nishide H., Ohyanagi M. *J. Phys. Chem.*, **1988**, *92*, 641.
43. Nishide H., Suzuki T., Soejima Y., Tsuchida E. *Macromol Chem. Symp.*, **1994**, *80*, 145.
44. Jones R. D., Summerville D. A., Basolo F. *Chemical Reviews*, **1979**, 2, 139.
45. Nishide H., Yoshioka H., Wang S. G., Tsuchida E. *Makromol. Chem.* **1985**, *186*, 1513.
46. Fallab S. *Angew. Chem. Int. Ed. Engl.* **1967**, *6*, 496.
47. *Chem. Eng. News*, **2002**, June 24.
48. Drioli E., Romano M. *Ind. Eng. Chem. Res.*, **2001**, *40*, 1277.

49. Baker W. R. *Ind. Eng. Chem. Res.*, **2002**, *41*, 1393.
50. Toshima N. *Polym. Gas Sep*., **1992**, *1*, 3.
51. Nishide H., Tsuchida E. *Polymer for Gas Separation*, Toshima N. ed. VCH Publishers: New York, 1992.
52. Aoki T. *Prog. Polym. Sci.*, **1999**, *24*, 951.
53. Stern S. A. *J. Membr. Sci.*, **1994**, *94*, 1.
54. Asakawa S., Saitou Y., Kawato M., Itoh Y., Tsuchiya S., Kanda K. *Natl Tech Report* **1983**, *29*, 93.
55. Houston K. S., Weinkauf D. H., Stewart F. F. *J. Membr. Sci.*, **2002**, *205*, 103.
56. Ichiraku Y., Stern S. A., and Nakagawa T. *J. Membr. Sci.*, **1987**, *34*, 5.
57. Tsuchihara K., Masuda K., Higashimura T. *Macromolecules*, **1992**, *25*, 5816.
58. Aoki T., Nakahara H., Oikawa E. *Polym. Prepr. Jpn.*, **1993**, *42*, 4036.
59. Nagase Y., Ochiai J., Matsui K., Uchida M. *Polymer*, **1988**, *29*, 740.
60. Kita H., Shigekuni M., Kawafune I., Kanaka K., Okamoto K. *Polym. Bull.*, **1987**, *21*, 371.
61. Freeman B. D. *Macromolecules*, **1999**, *32*, 375.
62. Way J. D., Noble R. D. *Membrane Handbook*; Sirkar K. K., Ho W. S. Ed. Van Nostrand Reinhold: New York, **1993**.
63. Scholander P. F. *Science*, **1960**, *132*, 585.
64. Wittenberg J. B. *J. Biol. Chem.*, **1966**, *241*, 104.
65. Basset R. J., Schultz J. S. *Biochim. Biophys. Acta*, **1970**, *211*, 194.
66. Paul D. R., Koros W. J. *J. Polym. Sci.: Polym. Phys. Ed.*, **1976**, *14*, 675.
67. Barrer R. M. *J. Membr. Sci.*, **1984**, *18*, 25.
68. Cussler E. L., Aris R., Brown A. *J. Membr. Sci.*, **1989**, *43*, 149.
69. Noble R. D. *J. Membr. Sci.*, **1992**, *75*, 121.
70. Hong S. U., Won J., Park H. C., Kang Y. S. *J. Membr. Sci.*, **1999**, *163*, 103.
71. Nishide H., Ohyanagi M., Okada O., Tsuchida E. *Macromolecules* **1987**, *20*, 417.
72. Nishide H., Kawakami H., Suzuki T., Azechi Y., Soejima Y., Tsuchida, E. *Macromolecules* **1991**, *24*, 6306.
73. Merkel T. C., Freeman B. D., Spontak R. J., He Z., Pinnau I., Meakin P., Hill A. J. *Science*, **2002**, *296*, 519.
74. Maja M., Orechia C., Strano M., Tosco P., Vanni M. *Electrochimica Acta*, **2000**, *46*, 423.
75. DeMarinis M., DeCastro E. *USP* 6, 103, 077 (**2000**).
76. Doughty D. H., Nazar L. F., Arakawa M., Brack H., Naoi K. *New Materials for Batteries and Fuel Cells*, Symposium held in April 5-8, 1999, San Francisco, CA, USA.

77. Jorissen L., Gogel V., Kerres J., Garche J. *J. Power Sources*, **2002**, *105*, 267.
78. Li Q., Bjerrum N. J. *J. Power Sources*, **2002**, *110*, 1.
79. Goldthan J., Brown I., Koretz B. *J. Power Sources*, **1999**, *80*, 171.
80. Kinoshita K. *Electrochemical Oxygen Technologies*, Wiley, New York, **1992**.
81. Holzer F., Muller S., Haas O. *J. Power Sources*, **1997**, *65*, 276.
82. Vielsticgich W. *Fuel cells*, Willy, London **1965**, p501.
83. Joon K. *J. Power Sources*, **1998**, *71*, 12.
84. Larminie J., Dicks A. L. *Fuel Cells Systems Explained*, Wiley, New York, **2000**.
85. Yeager E. *J. Mol. Catal.*, **1986**, *38*, 5.
86. Carrette L., Friedrich K. A., Stimming U. *Fuel Cells*, **2001**, *1*, 5.
87. Koper M. T. M. *J. Phys. Chem.*, **1997**, *B101*, 3168.
88. Kaifer A. E., Kaifer M. G. *Supramolecular Electrochemistry*, Weinheim, Wiley-VCH, **1999**.
89. Wei Z., Huang W., Zhang S., Tan J. *J. Power Sources*, **2000**, *91*, 83-85.
90. Lamminen J., Kivisaari J., Lampinen M. J., Viitanen M., Vuorisalo J. *J. Electrochem. Soc*., **1991**, *138*, 905.
91. Singhal S. C. *Solid State Ionics*, **2000**, *135*, 305.
92. Lamminen J., Kivisaari J., Lampinen M. J., Viitanen M., Vuorisalo J. *J. Electrochem. Soc*., **1991**, *138*, 905.
93. Yoshino M., Noya S., Hanabusa A., Yanagihara N. *JP* 04 02 046 (**1992**).
94. Hanabusa A., Noya S., Yoshino M., Yanagihara N. *JP* 04 17 259 (**1992**).
95. Sammels A. F., Schwartz, M. 3rd International Conference on *Catalysis in Membrane Reactors*, Copenhagen, Denmark, September **1998**.
96. *JP* 03-276576 (**1991**).
97. *JP* 6-140067 (**1994**).
98. *JP* 04-190570 (**1992**).
99. Nitta S., Taki M., Kawahara T., Miura M. *USP* 6, 106, 963 (**2000**).